Inorganic Chemistry

Article

pubs.acs.org/IC

Synthesis, Structure, Magnetic Behavior, and Theoretical Analysis of Diazine-Bridged Magnetic Ladders: Cu(quinoxoline)X_2 and Cu(2,3-dimethylpyrazine)X_2 (X = Cl, Br)

Joaquim Jornet-Somoza, Núria Codina-Castillo, Mercè Deumal,* Fernando Mota, and Juan J. Novoa

Departament de Química Física & IQTCUB, Universitat de Barcelona, Martí i Franquès 1, 08028-Barcelona, Spain

Robert T. Butcher and Mark M. Turnbull*

Carlson School of Chemistry and Biochemistry, Clark University, 950 Main St., Worcester, Massachusetts 01610, United States

Brian Keith and Christopher P. Landee

Department of Physics, Clark University, 950 Main St., Worcester, Massachusetts 01610, United States

Jan L. Wikaira

Department of Chemistry, University of Canterbury, Private Bag 4800 Christchurch, New Zealand

Supporting Information

ABSTRACT: The synthesis, structure, and magnetic behavior of the complexes Cu(qnx)Br_2 (**1**), Cu(2,3-dmpz)Br_2 (**2**), Cu(qnx)Cl_2 (**3**), and Cu(2,3-dmpz)Cl_2 (**4**) (qnx = quinoxaline, dmpz = dimethylpyrazine) are described. Both X-ray structural data and fitting of the magnetic data suggest that the compounds are well-described as strong-rung, two-leg magnetic ladders with J_{rung} ranging from −30 K to −37 K, and J_{rail} ranging from −14 K to −24 K. An unexpected decrease in the exchange constant for J_{rail} (through the diazine ligand) is observed when the halide ion is changed from bromide to chloride, along with a small decrease in the magnetic exchange through the halide ion. Theoretical calculations on **2** and **4** via a first-principles bottom-up approach confirmed the description of the complexes as two-leg magnetic ladders. Furthermore, the calculations provide an explanation for the experimentally observed change in the value of the magnetic exchange through the dmpz ligand when the halide ion is changed from bromide to chloride, and for the very small change observed in the exchange through the different halide ions themselves via a combination of changes in geometry, bond lengths, and anion volume.

INTRODUCTION

A molecular crystal will behave macroscopically as a magnetic material if, and only if, the magnetic interactions between radicals can propagate in one, two, or three directions. If they propagate over only one or two directions of space, the system is referred to as a low-dimensional magnet, to distinguish it from bulk magnetic compounds. There has been extensive study of a variety of low-dimensional molecular magnetic lattices over the past several decades.[1] Among these lattices, there has been particular interest in magnetic ladders, which is a topology where interactions between radicals propagate in two directions as follows: n radical chains of length L interact magnetically to generate an $n \times L$ system also known as an n-leg ladder. The magnetic interactions within one of the n chains are known as J_{rail}, and magnetic interactions between chains are known as J_{rung}. In the simplest case, two magnetic chains ($n = 2$; with interaction J_{rail}) are linked together by a single J_{rung} interaction to make a two-leg ladder.

The interest in these materials is due, in large part, to the existence of an energy gap in the spin excitation spectrum for even-legged ladders[2] and, as a result, to their relationship to other systems with such a gap,[1c] including Haldane chains.[3] Further interest in magnetic ladders comes from their relationship to certain phases of high-temperature superconductors.[4] The ladders themselves are also known to undergo a superconducting transition when doped.[5]

Among the best-studied spin ladders are the copper oxide-derived systems.[5,6] However, the very strong exchange observed in these materials makes it difficult to study them in their disordered state, or in applied fields that constitute a significant fraction of the critical field, again leaving the material in the singlet ground state. Molecular spin ladders, on the other hand, have the advantage of weaker interactions, which allows experiments in all regions of the magnetic excitation spectrum. These systems also are more readily adjusted through chemical modification of the ancillary portions of the structure, allowing for tuning of the interactions with respect to both the strength and sign of the magnetic exchange.

Received: March 8, 2012
Published: May 23, 2012

   dx.doi.org/10.1021/ic3005147 | *Inorg. Chem.* 2012, 51, 6315−6325

A small number of purely organic magnets with probable spin ladder structures have been reported,[7] along with a family of hybrid metal−organic compounds that derived their magnetic properties from the organic component.[8,9] A somewhat larger number of coordination compounds exhibiting spin-ladder magnetic behavior and owing the source of their magnetic moment to the metal species have been reported. These include several copper(II) complexes in which the spin ladder motif results from the crystal packing of CuX_4^{2-} ions,[10−13] and complexes where the spin ladder structure results from bridging metal species with diamagnetic ligands.[14−16]

Recent experience shows that the magnetic behavior of a compound may be more complex than first suggested by knowledge of the crystal structure.[17] The dominant interactions may occur in directions different from those showing the shortest inter-radical distances and/or the interladder interactions may not be negligible. The extensively studied vanadium compound $(VO)_2(P_2O_7)$ was originally interpreted as a two-leg spin ladder.[18−20] However, subsequent neutron scattering experiments showed that the principal magnetic interactions were those of an alternating chain oriented perpendicular to the structural ladder motif.[21,22] Other problems result when the symmetry of the system is lower than that of the ideal ladder, which would have only two different exchange pathways. For example, the copper complex Cu_2(1,4-diazacycloheptane)Cl_4 was initially reported and studied as a spin ladder,[16,23−25] but subsequent studies indicated that the system is more complex, with at least five different exchange pathways, and that its consideration as a spin ladder is an oversimplification.[26,27]

We have been interested in designing a series of magnetic ladders in the limiting cases of strong rung exchange and strong rail exchange, as well as isotropic systems. Thus, we have prepared several compounds that appear structurally as two-leg ladders and whose magnetic behavior agrees with that analysis using both the crystal packing and bridging ligand techniques.[10,12,14,15,28,29] In some cases, the properties have also been rationalized at the theoretical level.[10,29] In this general area, we have previously reported[14,15] the structures and magnetic susceptibility for Cu(qnx)Br_2 (**1**) and Cu(2,3-dmpz)Br_2 (**2**) (qnx = quinoxaline; dmpz = dimethylpyrazine; see Figure 1 for the molecular unit of **2**), which crystallize as two-leg spin ladders where the Cu(II) ions are the source of the unpaired electron. The rungs of the ladder are formed by dibromide bridges and the rails are formed by the bridging diazines. Here we report the synthesis and structures of the corresponding chloride complexes, Cu(qnx)Cl_2 (**3**) and Cu(2,3-dmpz)Cl_2 (**4**), their magnetic behavior, a study of the impact of temperature on the crystallographic structures, and a comparative theoretical-experimental analysis of the magnetic properties of the chloro and bromo Cu(2,3-dmpz)X_2 complexes.

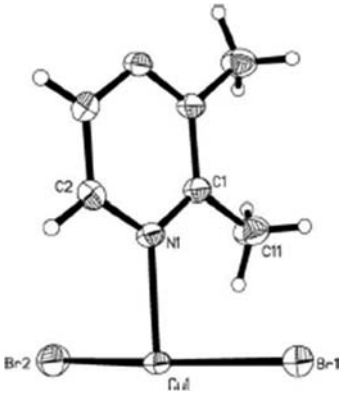

Figure 1. Molecular unit of Cu(2,3-dimethylpyrazine)Br_2 (**2**). Note that (**2**), and Cu(2,3-dmpz)Cl_2, (**4**) are isostructural compounds.

EXPERIMENTAL SECTION

1. Synthesis. Quinoxaline and 2,3-dimethylpyrazine were purchased from Aldrich Chemical Company and used as received. Copper(II) chloride dihydrate and copper(II) bromide were purchased from Aesar and used as received. Infrared (IR) spectra were recorded as KBr pellets on a Perkin−Elmer Model Paragon 500 or Spectrum 100 spectrophotometer (4000−450 cm^{-1}) and referenced to polystyrene.

Catena-quinoxalinedibromocopper(II) (**1**)[15] and *catena*-2,3-dimethylpyrazinedibromocopper(II) (**2**)[14] were prepared as previously reported.

The synthesis of *Catena*-quinoxalinedichlorocopper(II) (**3**) has been previously reported by Lindros and Lumme.[30] Material for both magnetic measurements and X-ray diffraction (XRD) was prepared via slow evaporation. A solution of $CuCl_2$ dihydrate [40 mL, 0.1 M in EtOH] was placed in a 50-mL beaker. A separate 50-mL beaker was filled with 40 mL of a solution of quinoxaline [also 0.1 M in EtOH]. These beakers were placed in a larger container and the outer container slowly filled with ethanol until the level of ethanol was 5 cm above the level of the smaller beakers. The outer container was sealed and the system left for approximately one month during which time small crystals grew from the diffusing mixture. The residual liquid was carefully removed, and the product harvested by filtration, washed with ethanol and air-dried to give green crystals, 0.46 g (43%). IR (KBr): ν 3102(w), 3067(w), 3045(w), 1508(s), 1466(m), 1358(s), 1214(m), 1210(m), 1145(s), 1140(s), 1056(s), 971(m), 876(m), 756(s), 644(w) cm^{-1}.

Catena-2,3-dimethylpyrazinedichlorocopper(II) (**4**) involved the addition of a solution of $CuCl_2 \cdot 2H_2O$ (0.336 g, 1.97 mmol) in 3:1 methanol/$CHCl_3$ to a stirred solution of 2,3-dmpz (0.217 g, 2.00 mmol) in 3:1 methanol/$CHCl_3$, which resulted in the immediate precipitation of a turquoise powder. After stirring for 10 min, the precipitate was isolated by filtration, washed with 50 mL of fresh 3:1 methanol/$CHCl_3$, and dried under vacuum to give 0.485 g (84.5%). IR (KBr): 3094(m), 1438(m), 1405(m), 1376(w), 1188(s), 1166(s), 852(m) cm^{-1}. Single crystals suitable for XRD analysis were grown by slow diffusion of a layered solution of $CuCl_2$ in water over 2,3-dmpz in CH_2Cl_2. IR (KBr): ν 3094(w), 1438(m), 1405(m), 1376(w), 1257(w), 1188(s), 1166(s), 1105(w), 1012(w), 973(w), 852(m), 758(w), 527(w) cm^{-1}.

2. X-ray Crystallography. Data for **1** and **3** were recorded with a Rigaku-Spider X-ray diffractometer, which was comprised of a Rigaku MM007 microfocus copper rotating-anode generator, high-flux Osmic monochromating and focusing multilayer mirror optics (Cu K radiation, λ = 1.5418 Å), and a curved image-plate detector. CrystalClear software[31] was utilized for data collection and FSProcess in PROCESS-AUTO software[32] was used for cell refinement and data reduction. Crystals of **4** were mounted on a Bruker/Siemens SMART system using φ and ω scans for data collection. Cell parameters were determined using SMART[33] software and refined using SAINTPlus.[34] Data reduction and corrections were performed using SAINTPlus.[34] Absorption corrections were made via SADABS.[35] All structures were solved employing direct methods and expanded by Fourier techniques.[36] Nonhydrogen atoms were refined anisotropically. Hydrogen atoms were placed in calculated positions and refined using a riding model with fixed isotropic *U* values. Details of the data collection parameters and the crystallographic information are provided in Table 1, while selected bond lengths and angles are given in Table 2, along with previously reported data for **1**−**4**. The new crystal data have been deposited with the CCDC (**1**, No. 826786; **3**, No. 826785; **4**, No. 826787). A Bruker D8 powder X-ray

dx.doi.org/10.1021/ic3005147 | Inorg. Chem. 2012, 51, 6315−6325

Table 1. New Crystallographic Data for Compounds Cu(qnx)Br_2 (1), Cu(qnx)Cl_2 (3), and Cu(2,3-dmpz)Cl_2 (4)

	1	3	4
empirical formula	$C_8H_6Br_2CuN_2$	$C_8H_6Cl_2CuN_2$	$C_6H_8Cl_2CuN_2$
formula weight	353.51	264.59	242.58
temperature (K)	138(2)	113(2)	93(2)
wavelength (Å)	1.54178	0.71073	0.71073
crystal system	monoclinic	monoclinic	monoclinic
space group	*C*2/*m*	*C*2/*m*	*C*2/*m*
unit-cell dimensions			
a (Å)	13.1018(3)	13.1229(4)	12.8193(10)
b (Å)	6.95350(10)	6.9476(2)	6.9031(5)
c (Å)	10.3240(7)	9.7058(3)	9.5759(7)
β (°)	107.547(8)	107.467(2)	105.982(3)
volume (Å^3)	896.79(7)	844.10(4)	814.65(11)
Z	4	4	4
density (calculated, Mg/m^3)	2.618	2.082	1.978
absorption coefficient (mm^{-1})	13.443	3.161	3.265
F(000)	668	524	484
crystal size (mm^3)	0.19 × 0.04 × 0.01	0.68 × 0.34 × 0.13	0.50 × 0.30 × 0.20
data collection range, *θ* (deg)	3.55−31.51	3.25−27.57	3.38−22.71
index ranges	$-15 \le h \le 13$	$-16 \le h \le 16$	$-13 \le h \le 12$
	$-8 \le k \le 7$	$-8 \le k \le 9$	$-7 \le k \le 7$
	$-11 \le l \le 11$	$-12 \le l \le 12$	$-9 \le l \le 10$
reflections collected	4737	8164	1386
independent reflections	792 [*R*(int) = 0.1133]	1047 [*R*(int) = 0.0193]	575 [*R*(int) = 0.0182]
completeness (%)	99.9	99.3	95.4
absorption correction		semiempirical from equivalents	
refinement method		full-matrix least-squares on F^2	
data/restraints/parameters	792/12/64	1047/0/64	575/0/56
goodness-of-fit on F^2	1.132	1.110	1.214
final *R* indices [$I > 2\sigma(I)$]			
*R*1[a]	0.0613	0.0187	0.0259
*w*R2[a]	0.1592	0.0531	0.0709
R indices (all data)			
*R*1[a]	0.0685	0.0195	0.0260
*w*R2[a]	0.2062	0.0537	0.0709
largest diff. peak and hole	1.888 and −1.653 e Å^{-3}	0.490 and −0.317 e Å^{-3}	0.626 and −0.443 e Å^{-3}

[a] $R_1 = \sum||F_0| - |F_c||/\sum|F_0|$; $wR_2 = \{\sum[w(F_0^2 - F_c^2)^2]/\sum[w(F_0^2)^2]\}^{1/2}$.

Table 2. Selected Bond Lengths and Angles for Compounds 1−4, at Their Indicated Temperatures[a]

	1		2	3		4
	304 K (ref 15)	138 K (this work)	295 K (ref 14)	295 K (ref 30)	113 K (this work)	93 K (this work)
			Bond Lengths (Å)			
Cu1−X1	2.4285(6)	2.438(2)	2.442(1)	2.300(2)	2.3062(6)	2.3138(13)
Cu1−X1A	2.9162(6)	2.898(2)	2.9011(12)	2.685(1)	2.6605(6)	2.6474(12)
Cu1−X2	2.3702(6)	2.377(2)	2.3833(10)	2.232(2)	2.2369(6)	2.2458(12)
Cu1−N1	2.0610(19)	2.090(7)	2.057(4)	2.068(2)	2.0676(14)	2.065(3)
			Bond Angles (deg)			
Cu1−X1−Cu1A	90.473(18)	90.05(7)	92.02(3)	91.47(4)	90.70(2)	91.57(4)
N1B−Cu1−N1	174.16(11)	175.0(4)	173.2(2)	174.07(8)	174.42(7)	173.54(15)
N1−Cu1−X2	88.85(6)	88.88(18)	88.73(10)	88.89(5)	88.94(4)	88.72(7)
N1−Cu1−X1	90.50(6)	90.52(19)	90.56(10)	90.41(4)	90.35(4)	90.54(7)
X2−Cu1−X1	166.72(2)	165.70(10)	167.56(5)	166.04(3)	165.00(3)	166.30(5)
N1−Cu1−X1A	92.88(5)	92.5(2)	93.38(11)	92.95(5)	92.77(4)	93.20(7)
X2−Cu1−X1A	103.76(2)	104.35(8)	104.46(4)	105.43(4)	105.70(2)	105.27(4)
X1-Cu1−X1A	89.527(18)	89.95(7)	87.98(3)	88.53(4)	89.30(2)	88.43(4)
C2−N1−C3	116.9(2)	117.9(7)	117.9(4)	117.4(2)	117.31(14)	117.9(3)
C2−N1−Cu1	119.93(16)	120.6(5)	118.6(3)	119.62(9)	119.78(10)	118.8(2)
C3−N1−Cu1	123.12(16)	121.5(5)	123.5(3)	122.96(10)	122.88(10)	123.3(2)

[a] Symmetry transformations: A = $-x, -y, -z$; B = $x, -y, z$.

dx.doi.org/10.1021/ic3005147 | *Inorg. Chem.* 2012, 51, 6315−6325

diffractometer was used to verify that powder samples used for magnetic measurements were the same phase as the single crystal.

3. Magnetic Data Collection. Magnetic susceptibility data for compounds **1**−**4** were measured on a Quantum Design MPMS-XL SQUID magnetometer. Crystals of **1**−**4** were powdered and packed into #3 gelatin capsules. There was no hysteresis observed in the magnetization of the sample as a function of applied field, from 0 to 50 kOe at 1.8 K. The moments were linear with the applied field up to at least 5000 Oe. Susceptibility data were taken over the temperature range from 1.8 K to 310 K in an applied field of 1000 Oe. The data were corrected for temperature-independent paramagnetism of the Cu(II) ion and for the diamagnetism of the constituent atoms using Pascal's constants. The data were fitted to the appropriate analytical function[37] to extract fitting J_{AB} parameters, using the Hamiltonian in eq 1:

$$\hat{H} = -2 \sum_{A,B} J_{AB} \hat{S}_A \cdot \hat{S}_B \quad (1)$$

4. Theoretical Methods. The first-principles bottom-up procedure[38] was employed to gain a rigorous and properly founded understanding of the magnetic properties of compounds **2** and **4**. This procedure is a four-step working strategy that allows the computation of the macroscopic magnetic properties with the only input being the experimental crystal structure (at a representative temperature). No assumptions of any type are made concerning the sign or size of the radical···radical magnetic interactions present in the crystal. The four steps involved in the procedure are as follows: (1) identification of all unique radical···radical pairs present in the crystal, (2) calculation of the radical···radical magnetic interactions (J_{AB}) for all unique pairs, (3) determination of the magnetic topology of the crystal and the finite minimal magnetic model, and (4) calculation of the macroscopic magnetic properties of the crystal.

Identification of All Unique Radical···Radical Pairs Present in the Crystal. This analysis was carried out on all crystals of interest. All symmetry-unique radical···radical pairs whose distance is smaller than a given threshold (selected in such a way that all relevant first- and second-nearest-neighbors radical···radical pairs are included) were considered in the analysis. As it will be shown below, because of the two-leg structure of these crystals, some radical···radical pairs present through-bond magnetic interactions while others present through-space interactions.

Calculation of the Radical···Radical Magnetic Interactions (J_{AB}) for All Unique Pairs. The J_{AB} in crystals **2** and **4** formally originates in the Cu(II) ions and the ligands are all diamagnetic. In order to reproduce the electronic structure of the interacting electrons properly, each Cu(II) radical will be coordinated with all its linked ligands, that is, each radical in $Cu(2,3\text{-dmpz})_2Br_2$ will be constituted by one Cu(II), two (2,3-dmpz) ligands, and two Br ligands in equatorial positions, at their geometry in the crystal. For each pair of coordinated Cu(II) radicals, J_{AB} can be obtained as $J_{AB} = [E^S_{BS} - E^T]$,[39] where the open-shell singlet E^S_{BS} is computed using the *broken-symmetry* (BS) approximation[40] at the UB3LYP DFT level,[41,42] as implemented in Gaussian 03[43] and the following basis sets: Ahlrich's DZP[44] on Cu and the 6-31+G(d)[45] on the remaining atoms. This expression assumes that the overlap between SOMO orbitals on radicals A and B is small, which is true in most through-space interactions and in some through-bond magnetic interactions. Energy values and, in turn, J_{AB} values have an accuracy of 10^{-7} au ($0.05\ cm^{-1}$).

Determination of the Magnetic Topology of the Crystal and the Finite Minimal Magnetic Model. The magnetic topology is straightforwardly defined by looking at the network of connectivities among the spin centers that make the non-negligible J_{AB} interactions. Previous tests have shown that, when $|J_{AB}| < 0.05\ cm^{-1}$, the magnetic interaction can be considered as negligible.

Once the magnetic topology of the crystal is defined, the minimal magnetic model comprises the smallest group of radicals whose propagation along the three crystallographic axes reproduces the magnetic topology of the infinite crystal in an even way. It should include all significant J_{AB} magnetic interactions in a proportion as close as possible to that found in the infinite crystal. Larger models can also be obtained by extending the minimal magnetic model. However, if the minimal magnetic model is properly defined, the macroscopic properties computed should converge toward the experimental data as the minimal magnetic model is enlarged.

Calculation of the Macroscopic Magnetic Properties of the Crystal. The matrix representation of the Heisenberg Hamiltonian (defined in eq 1) in the space of all eigenstates of the minimal magnetic model space is uniquely defined when all of the J_{AB} values are computed. These values were computed in step 2 and the model space is defined in Step 3. The size of the matrix representation increases with the number n of doublet radical centers as $n!/[(n/2)!(n/2)!]$. In practice, this means that we are computationally limited to models of 16 spin centers or fewer. Finally, it is worth pointing out here that we have used the form of the Heisenberg Hamiltonian given in eq 2, which results in the same energy differences between eigenvalues as those obtained using the more common expression given in eq 1. Since the energy differences represent the relevant result when computing any of the macroscopic magnetic properties, the results obtained using the eigenvalues from eqs 1 or 2 are the same, and this is true for any macroscopic magnetic property (magnetic susceptibility, heat capacity, magnetization, etc.). Note that in eqs 1 and 2, $\hat{S}_A$ and $\hat{S}_B$ are the total spin operators acting on radicals A and B, and $\hat{I}_{AB}$ is the identity operator.

$$\hat{H} = -2 \sum_{A,B} J_{AB} \left(\hat{S}_A \cdot \hat{S}_B + \frac{1}{4} \hat{I}_{AB} \right) \quad (2)$$

As a final remark, the procedure is called *bottom-up* because the macroscopic magnetic properties are obtained from the microscopic radical···radical magnetic interactions without any prior assumptions about the size or topology of the magnetic interactions acting in the crystal. It is also a *first-principles* procedure because the J_{AB} magnetic interaction for each pair is obtained from energy differences between states computed by first-principles methods (high-level ab initio[46] or DFT methods[41]).

RESULTS AND ANALYSIS

1. Synthesis and Structure. Reaction of copper(II) chloride or bromide with quinoxaline (qnx) or 2,3-dimethylpyrazine (2,3-dmpz) in alcoholic solution gave the corresponding complexes $Cu(qnx)Br_2$ (**1**), $Cu(2,3\text{-dmpz})Br_2$ (**2**), $Cu(qnx)Cl_2$ (**3**), or $Cu(2,3\text{-dmpz})Cl_2$ (**4**) in 40%−80% yield, all of which present a ladder motif in their crystal packing. High yields were obtained when solutions of the two reagents were mixed directly, resulting in an insoluble powder. Diffusion methods were used to obtain single crystals suitable for X-ray diffraction (XRD). Single-crystal XRD data were collected for compound **4** and new low-temperature data sets were obtained for the previously reported compounds **1**[15] and **3**.[30]

New crystal structure data and refinement parameters for **1**, **3**, and **4** are given in Table 1, while bond lengths and angles for **1**−**4** at varying temperatures are given in Table 2. All four complexes crystallize in the monoclinic space group $C2/m$. (Only figures for **4** are shown. A view of **4** with thermal ellipsoids is shown in Figure 2.)

The four complexes crystallize forming the same structural ladder motif (see Figure 2). The rungs of these ladders are formed by bihalide bridges (bromide ions for **1** and **2**, chloride ions for **3** and **4**). The rails are formed by bridging diazine molecules (quinoxaline for **1** and **3**, 2,3-dimethylpyrazine for **2** and **4**). Adjacent ladders are separated by the alkyl groups or aromatic rings parallel to the *c*-axis (see Figure 3a). Although the possibility of significant interactions mediated by the two-halide exchange pathway[47] exists between ladders, these are not anticipated to be significant here. Adjacent ladders along the *a*-axis are offset by 1/2-unit cell (parallel to the *b*-axis) reducing

dx.doi.org/10.1021/ic3005147 | Inorg. Chem. 2012, 51, 6315−6325

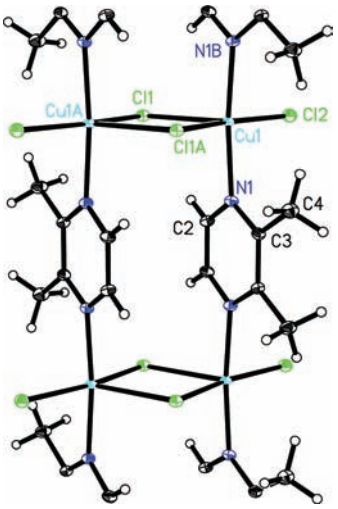

Figure 2. Thermal ellipsoid plot of Cu(2,3-dmpz)Cl_2 (**4**) showing the ladder structure. Only the non-hydrogen atoms in the asymmetric unit and Cu coordination sphere have been labeled.

the significance of interladder interactions via halide···halide contacts, as a result of symmetry cancellation, X···X distances, and Cu−X···X bond angles[48] (see Figure 3b and the Theory section for the calculated interladder exchange values).

2. The Impact of Thermal Expansion on the Crystal Structures. The temperature at which the crystal has been determined in XRD can be very relevant when the thermal expansion of the crystal presents non-negligible magnetic effects. Consequently, we explored these thermal effects in the structures of **1** and **3**.

Comparison of the unit-cell parameters between room-temperature (RT) and low-temperature (LT) data shows very small, but anisotropic, changes (the *b*-axis expands while the *a*- and *c*-axes contract). In compound **1**, the cell parameters are (RT/LT) a = 13.175(2) Å/13.102(3) Å, b = 6.929(1) Å/6.954(1) Å, c = 10.356(1) Å/10.324(1) Å, β = 107.70(1)°/107.55(1)°, V = 900.7(2) $Å^3$/896.8(1) $Å^3$, while for compound **3**, they are a = 13.237(5) Å/13.123(1) Å, b = 6.935(3) Å/6.948(1) Å, c = 9.775(3) Å/9.706(1) Å, β = 107.88(2)°/107.47(1)°, V = 853.9(5) $Å^3$/844.1(1) $Å^3$. This is only a 0.4% decrease in the volume of **1** and a 1.1% decrease in the volume of **3**. All cell parameters decrease at low temperature except for the *b*-axis (ladder axis) length, which shows a very small (∼0.2%) increase. The corresponding change in bond lengths and angles within the complexes are equally small (the maximum change in Cu−N or Cu−X bond length is 0.03 Å; see Table 2), suggesting very little change in the structure of the ladders or the interladders disposition, as a function of temperature. The slight expansion of the unit cell parallel to the *b*-axis (the rail spin-ladder axis) upon cooling in compounds **1** and **3** is somewhat unusual. Examination of bond parameters along this axis in **1** indicates that the Cu−N bond has lengthened slightly (from 2.061(2) Å at RT to 2.090(7) Å at 138 K), but this is partially compensated for by a compression of the quinoxaline ring itself ($d_{N\cdots N}$ = 2.813(2) Å at RT, but is shortened to 2.777(5) at 138 K). The expansion is even smaller in **3** where the *b*-axis lengthens by <0.02 Å. Here, although the Cu−N bonds are identical, within error, the quinoxaline ring expands slightly ($d_{N\cdots N}$ = 2.805(3) Å at room temperature, 2.817(5) at 113 K). In both compounds, the Cu−X1−Cu bridging angle is compressed at low temperature, bringing the quinoxaline rings slightly closer together and increasing the steric hindrance between them. The Cu···Cu distance (via a combination of change in the Cu−N bond and quinoxaline ring) increases along the *b*-axis, to compensate for the increase in crowding.

3. Magnetic Data. Magnetic susceptibility data (Figure 4) were collected as a function of temperature for powder samples of **1**−**4** from 1.8 K to 310 K. All four compounds exhibit a maximum in the magnetic susceptibility in the range of 20−30 K, with the temperature of the maximum and value of χ at the maximum varying for each compound. The data could be fitted by a model for a strong-rung ($J_{rail} < J_{rung}$) two-leg ladder.[37] The fitting parameters are given in Table 3.[49] Note that, in light of the ab initio computations (as will be discussed later), there was no need to explore fitting the data with magnetic models other than the strong-rung spin ladder.

4. Theoretical Analysis of the Magnetic Properties of Cu(2,3-dmpz)Cl_2 and Cu(2,3-dmpz)Br_2. In order to improve our understanding of the magnetic properties of compounds **1**−**4**, a first-principles bottom-up analysis was done on two of the complexes: **2** (Cu(2,3-dmpz)Br_2) and **4** (Cu(2,3-

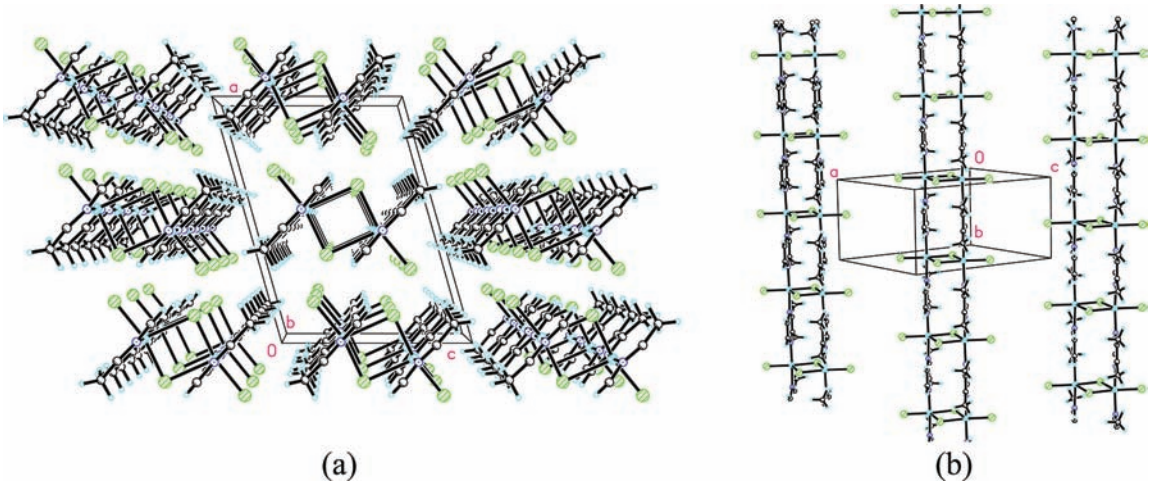

Figure 3. Crystal packing of compound **4**: (a) viewed parallel to the *b*-axis, showing the separation of the ladders; (b) viewed perpendicular to the ladder face, showing how adjacent ladders are offset by 1/2-unit cell parallel to the *b*-axis.

dx.doi.org/10.1021/ic3005147 | *Inorg. Chem.* 2012, 51, 6315−6325

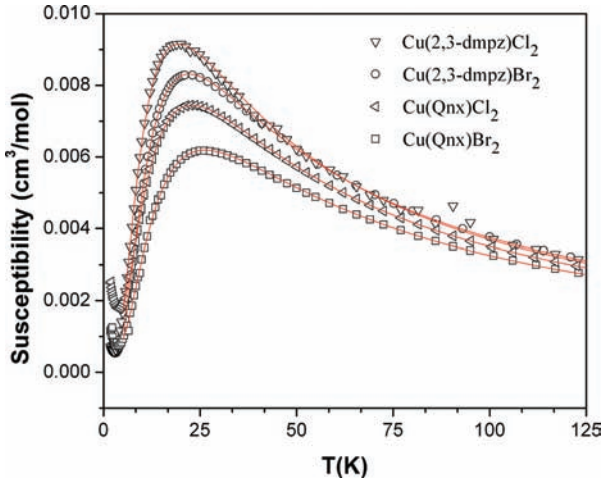

Figure 4. Molar susceptibility as a function of temperature for compounds **1**–**4**. The solid line represents the fit to a strong-rung two-leg ladder model.

Table 3. Fitted Magnetic Parameters for Compounds 1–4

compound	C (emu K mol^{-1} Oe^{-1})	$2J_{rung}/k$ (K)	$2J_{rail}/k$ (K)	impurity fraction
1	0.406(1)	−37.61(12)	−23.8(3)	0.0056(1)
2	0.427(8)	−31.75(1)	−18.39(2)	0.0031(1)
3	0.424(1)	−33.87(10)	−20.0(2)	0.012(2)
4	0.435(5)	−30.05(1)	−13.77(6)	0.0031(1)

dmpz)Cl_2), taken as prototypes of the Cl- and Br-substituted compounds. The results obtained in each of the four steps of the first-principles bottom-up analysis method are given hereafter grouped by steps.

Step 1: Identification of All Unique Radical···Radical Pairs Present in the Crystals of ***2*** *and* ***4****.* A comprehensive analysis of the crystals of **2** (Cu(2,3-dmpz)Br_2) and **4** (Cu(2,3-dmpz)Cl_2)) was done in order to identify all symmetry-unique radical pairs capable of presenting a non-negligible magnetic coupling between them, that is non-negligible J(di) interactions. The criterion used to decide which pairs of radicals to consider initially is the distance between spin-carrying groups, formally the Cu(II) atoms: all Cu(II)···Cu(II) pairs whose separation is <10 Å were initially considered (this cutoff criterion included all first- and second-nearest neighbors).

Eight radical pairs have a Cu(II)···Cu(II) distance of <10 Å in **2**, Cu(2,3-dmpz)Br_2; they are shown in Figure 5, with their Cu(II)···Cu(II) distance indicated in Table 4. Among these eight pairs, three of them (d1, d2, and d3) are intraladder. Note also that here d1 is the radical pair responsible for the rung interaction in the 2-leg ladder, d2 is responsible of the rail interaction, and d3 corresponds to a diagonal intrarail interaction connecting the two legs of the ladder (other symmetry-equivalent d1–d3 radical pairs in Figure 5a are not

Table 4. Values of the J(di) Magnetic Interactions (in cm^{-1}) for All Symmetry-Unique Radical Pairs Found in the Crystals of 2 and 4[a]

	Cu(2,3-dmpz)Br_2 (**2**)		Cu(2,3-dmpz)Cl_2 (**4**)	
	Cu···Cu (Å)	J(di) (cm^{-1})	Cu···Cu (Å)	J(di) (cm^{-1})
radical pair				
d1	3.858	−13.82	3.562	−14.23
d2	6.883	−10.26	6.903	−8.82
d3	7.890	−0.71	7.768	−0.73
d4	7.428	+0.84	7.280	+0.35
d5	6.589	+0.16	6.419	+0.13
d6	6.549	−1.05	6.241	−0.86
d7	9.501	−0.13	9.306	−0.11
d8	9.101	−0.01	9.090	+0.01
d9			9.496	+0.03
d10			9.576	+0.00
experimental fitting				
J_{rung}		−11.03		−10.44
J_{rail}		−6.39		−4.79

[a]The Cu(II)···Cu(II) distance is given for each pair. Fitting J parameters are also given for comparison purposes.[50]

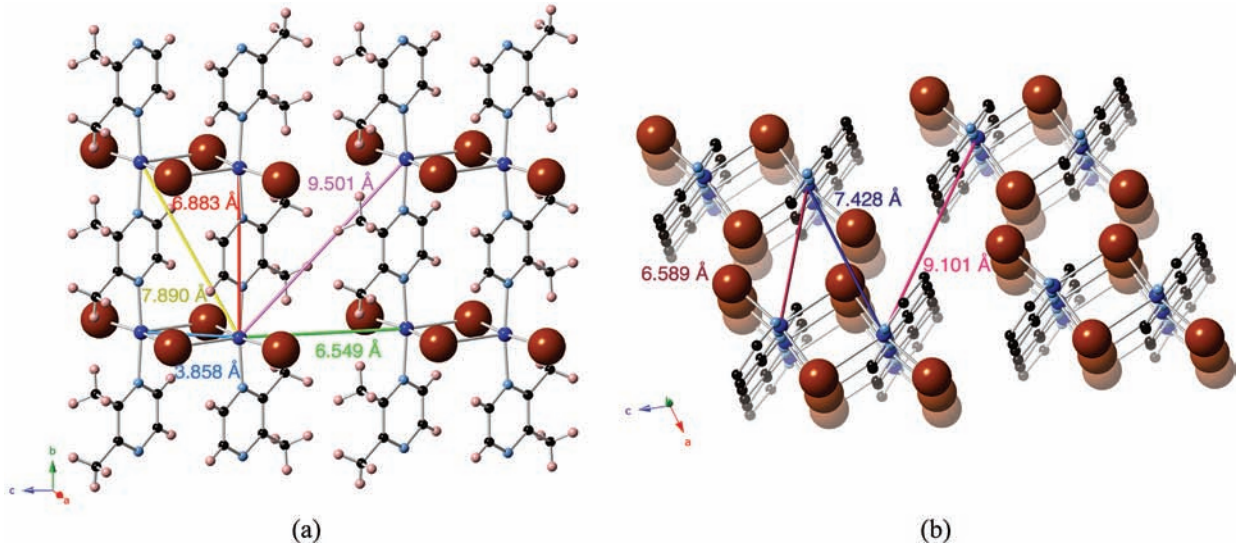

Figure 5. The eight symmetry-unique radical pairs found in the crystal of **2** (for each pair, the Cu(II)···Cu(II) distance is indicated in Ångstroms): (a) intraladder pairs (d1, d2, and d3 in Table 4) and interladder pairs along the *bc*-plane (d6 and d7 in Table 4); (b) interplane radical pairs (d4, d5, and d8 in Table 4). Note that, in panel b, hydrogen atoms have been removed, for the sake of simplicity.

dx.doi.org/10.1021/ic3005147 | *Inorg. Chem.* 2012, 51, 6315–6325

shown, for the sake of better clarity). Figure 5a also shows the two radical pairs that connect one 2-leg spin ladder with its adjacent one along the *bc*-plane, d6 and d7 (shown twice). Finally, Figure 5b shows the radical pairs that connect Cu(II) centers located in different *bc*-planes. It is also worth noting that, while d1 and d2 are through-bond magnetic interactions, all others are of the through-space type.

When a similar analysis is done on **4**, Cu(2,3-dmpz)Cl_2 (see Table 4 for Cu(II)···Cu(II) distances), three intraladder radical pairs were identified (d1, d2, and d3, with the same physical meaning as in **2**, and Cu···Cu distances 3.562, 6.903, and 7.768 Å) plus seven interladder radical pairs (d4−d10, with Cu···Cu distances, in increasing order, 6.241, 6.419, 7.280, 9.090, 9.306, 9.496, and 9.576 Å). Once again, d1 and d2 are the rung and rail magnetic interactions, respectively, both of the through-bond type, while all others are of the through-space type.

*Step 2: Calculation of the Radical···Radical Magnetic Interactions (J_{AB}) for All Unique Pairs of **2** and **4**.* For each radical-pair selected in Step 1, the value of the microscopic magnetic interaction, $J(\mathrm{d}i)$, was then computed. This magnetic coupling $J(\mathrm{d}i)$ is calculated from the energy difference between the open-shell singlet state and the triplet state, as indicated above (the Heisenberg Hamiltonian expression is that from eq 1). The broken symmetry approximation has been used to calculate the energy of the open-shell singlet states.[40]

The $J(\mathrm{d}i)$ results computed for all symmetry-unique radical pairs found in **2** and **4** are collected in Table 4. In both crystals, there are seven non-negligible radical pairs: d1−d7. Note that not all of them are antiferromagnetic, although the dominant ones have such character. Note also that the strength of each interaction is not always proportional to the Cu(II)···Cu(II) distance.

The pair approximation employed up to this point can sometimes be erroneous, bceause of the presence of polarization effects that radicals adjacent to the radical pair can induce on the radical pair. The possible existence of these polarization effects was checked by performing calculations using four-radical models on crystals of **4**, Cu(2,3-dmpz)Cl_2. It is found that the value of $J_{rung} = J(\mathrm{d1})$ varies from −14.23 cm^{-1} to −13.87 cm^{-1} when going from the dimer model to the tetramer model. On the other hand, $J_{rail} = J(\mathrm{d2})$ goes from −8.82 cm^{-1}, using a dimer model, to −8.52 cm^{-1}, for a tetramer model. It is obvious that individual J values will differ, depending on the model (**2** or **4** radicals) used to perform the ab initio computations. However, one must keep in mind that our objective is to reproduce experimental magnetic properties. Based on our experience in reproducing experimental $\chi(T)$ data in molecular magnetism, the key point in this procedure is not only the value of the computed microscopic magnetic exchange interactions, J, but the relative ratios between them: J_{rung}/J_{rail} = 1.6 for both dimer and tetramer models (see Figure S1 in the Supporting Information). Therefore, the dimer model works well in crystal **4**, and is also expected to work well in the dimers of crystal **2** studied here.

It is well-known that the least-squares functions used to fit the experimental data with the desired parameters could present multiple local minima. As mentioned in the Introduction, the magnetic behavior of a compound may be more complex than first suggested by knowledge of the crystal structure. Therefore, all theoretical ab initio calculations of microscopic J magnetic exchange interactions have been planned to get the right physical interpretation to the Cu(2,3-dmpz)X_2 systems **2** and **4**, and to finally assign the experimental fitting J_{rung} and J_{rail} parameters shown in Table 4 among different strong-rung spin-ladder models obtained in the fitting procedure. This example illustrates the relevance of computational chemistry methods as tools to theoretically discriminate which is the best fitting model to be used.

Step 3: Determination of the Magnetic Topology of the Crystal. The non-negligible $J(\mathrm{d}i)$ magnetic interactions define a topology consisting of a set of weakly interacting antiferromagnetic 2-leg spin ladders (the largest interladder interaction is ∼|1| cm^{-1} in both cases), where each 2-leg ladder has the properties of a strong-rung ladder (see Figure 6). It must be

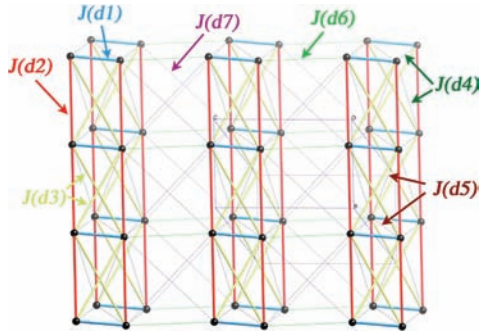

Figure 6. Magnetic topology of the Cu(2,3-dmpz)Br_2 crystal (**2**).

mentioned here that, although the computed values of J_{rung} are in good agreement with the experimentally fitted data (−13.82 cm^{-1} vs −11.03 cm^{-1} in **2**; −14.23 cm^{-1} vs −10.44 cm^{-1} in **4**), there is some numerical difference in the J_{rail} values (−10.26 cm^{-1} vs −6.39 cm^{-1} in **2**; −8.82 cm^{-1} vs −4.79 cm^{-1} in **4**). We emphasize here that the theoretical in-detail study of all exchange-pair interactions J_{AB} is intended to provide a complete picture of the microscopic magnetic pathways.

*Step 4: Calculation of the Macroscopic Magnetic Properties of the Crystal of **2** and **4**.* To obtain a proper estimate of the magnetic properties, one needs a magnetic model capable of reproducing the magnetic topology of the crystal as closely as possible. Such reproducibility can be tested by extending the magnetic model, as a proper magnetic model should show convergence in the computed magnetic properties (toward the experimental data) when it is extended.

To test the importance of the weak interactions between the two-leg ladders of the magnetic topology, we started using magnetic models made of isolated ladders (note that the largest interchain J_{AB} value is in the −1 cm^{-1} range, while the largest intrachain J_{AB} parameters are in the −14 cm^{-1} range, which is more than 10 times larger) (see Figure S2 in the Supporting Information). Afterward, we expanded the model by taking into account the interchain interactions and examining changes relative to the isolated two-leg spin-ladder model (see Figure S3 in the Supporting Information). All computed $\chi(T)$ curves reproduce the shape of the experimental curve well, and convergence is reached when using the eight-site model, which is therefore taken as the minimal magnetic model. The impact on the magnetic susceptibility curves of the interchain magnetic interactions was explored and we can conclude that, given their small magnitude, the weak interchain ladder interactions are not relevant in reproducing the macroscopic magnetic properties of Cu(2,3-dmpz)Br_2 (**2**). Therefore, this system may be safely considered as an isolated 2-leg spin-ladder magnet for simulation purposes. The same conclusions are

dx.doi.org/10.1021/ic3005147 | *Inorg. Chem.* 2012, 51, 6315−6325

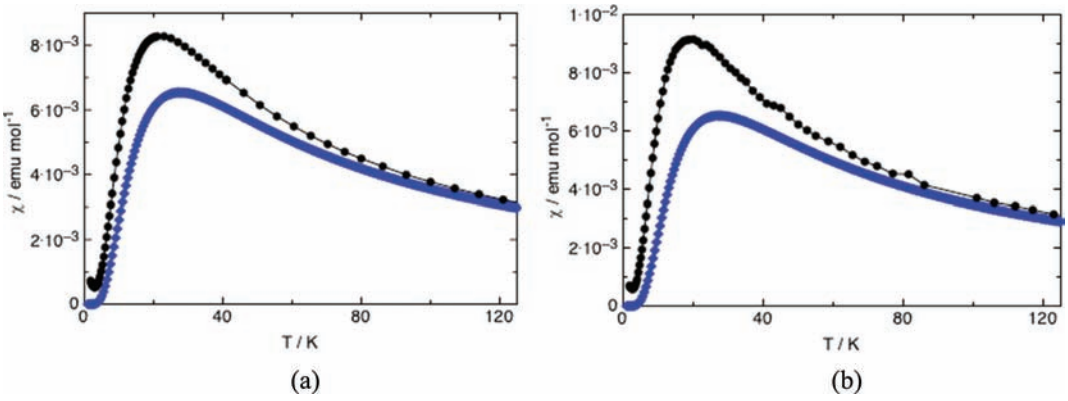

Figure 7. Comparison between experimental (in black) and computed magnetic susceptibility curves (in blue using a 8-radical model at 0 T), $\chi(T)$, for (a) Cu(2,3-dmpz)Br_2 (**2**), and (b) Cu(2,3-dmpz)Cl_2 (**4**) crystals.

reached when the magnetism of the Cu(2,3-dmpz)Cl_2 crystal (**4**) was studied using the first-principles bottom-up procedure, although we will not further discuss them. This conclusion further validates previous treatment of these complexes as isolated spin ladders.[14,15]

Figure 7 shows a comparison between both experimental and computed magnetic susceptibility curves for Cu(2,3-dmpz)Br_2 (**2**) and Cu(2,3-dmpz)Cl_2 (**4**) crystals, using the corresponding 8s minimal magnetic model.

Let us make a final comment on the fact that, for simulation purposes, often one does not use the magnetic model inferred directly from the calculated magnetic topology, but rather a more general model. The theoretical calculation of $\chi(T)$ is based on choosing the most appropriate magnetic model for simulation, which must be an agreement between model size and comprehensive description of the magnetic topology. Therefore, the choice of this general or coarse magnetic model depends on the ratio among microscopic J pair interactions, and thus one usually neglects $|J| < 10\%|J_{largest}|$. Accordingly, for the Cu(2,3-dmpz)X_2 system, the weakly interacting AFM two-leg spin-ladder magnetic model evolves into an AFM two-leg ladder model in order to calculate $\chi(T)$. One must obviously check that magnetic models with and without neglected Js converge toward the same $\chi(T)$ value, which must also agree with the experimental data.

5. A Comparative Study of the Magnetism in Cu(2,3-dmpz)Br_2 (2) and Cu(2,3-dmpz)Cl_2 (4). As a final step of this work, we investigated the similarities and differences between the bromide and chloride analogues, Cu(2,3-dmpz)Br_2 and Cu(2,3-dmpz)Cl_2 (**2** and **4**, respectively). As shown in Table 4 and Figure 6, both crystals have similar topology and $J(di)$ values, which correspond to a strong-rung two-leg spin-ladder system. Experimentally, the J_{rung}/J_{rail} relative strength is 1.73 for **2** and 2.18 for **4**, which should be respectively compared to theoretical values of 1.35 and 1.61. Interestingly, although the individual J_{rung} and J_{rail} values are different, the relative strength is maintained; both the experimental and computed J_{rung}/J_{rail} ratios are larger for the chloride compound. Therefore, when bromide is replaced by chloride, not only is the two-leg ladder magnetic topology preserved, but the dominant magnetic interactions (J_{rung} and J_{rail}) are preserved as well. This is at least partially a surprising conclusion, given the different properties of Cl and Br (electronegativity, polarizability, Cu-halogen distance). Thus, a more-detailed analysis became appropriate.

Let us begin by comparing the crystal packing of **2** and **4**. Figure 8 and Table 5 collect the most relevant distances (Cu−halogen, Cu−N, C_{arom}−C_{arom}), and a few relevant angles and torsion angles for the crystals of **2** and **4**. As expected, the chloride analogue (**4**) shows slightly shorter Cu−X distances, compared to the bromide analogue **2**, $|\Delta Cu{-}X| \approx 0.25$ Å. A very striking point is the way the Cu···Cu distance changes along the rung or rail (see Table 5). The Cu···Cu distance varies by 0.30 Å within the rung, while within rails, it only changes 0.02 Å (see Figure 8). The Cu−N(2,3-dmpz) distance is practically the same in **2** and **4**, and the same applies to the C_{arom}−C_{arom} distances within the 2,3-dmpz ring (Figure 8). The planarity of the 2,3-dmpz ring is also preserved (see Table 5 and Figure 9a for the atom numbering). There is also no

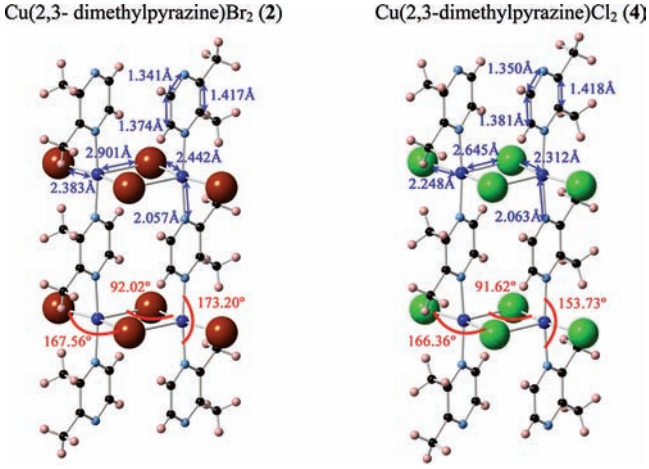

Figure 8. Comparison of the most relevant distances (in Ångstroms) and angles (in degrees) in the crystal packing of **2** (Cu(2,3-dmpz)Br_2) and **4** (Cu(2,3-dmpz)Cl_2).

Table 5. Value of the Cu···Cu Distance along the Rail and Rungs and of the Torsion Angles in the 2,3-dmpz Ring, for 2 and 4[a]

	Cu(2,3-dmpz)Cl_2 (**4**)	Cu(2,3- dmpz)Br_2 (**2**)
$d_{Cu\cdots Cu}$ (rung)	3.562 Å	3.858 Å
$d_{Cu\cdots Cu}$ (rail)	6.883 Å	6.903 Å
∠C3−C1−N−C2	2.82°	3.08°
∠C4−C2−N−C1	2.85°	3.11°

[a]See Figure 9a for atom numbering.

dx.doi.org/10.1021/ic3005147 | *Inorg. Chem.* 2012, 51, 6315−6325

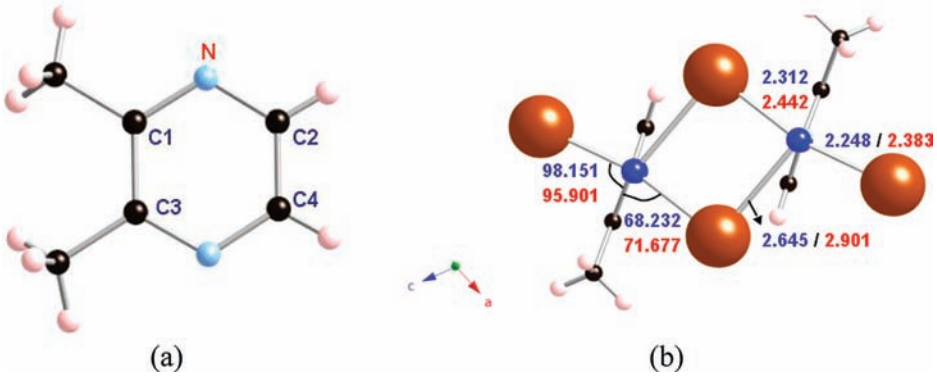

Figure 9. (a) Atom numbering used in Table 5 to represent the dihedral angles for the 2,3-dmpz ring. (b) Cu–halogen distances (in Ångstroms), angles and torsion angles between the plane of the 2,3-dmpz ring and the halogen bridge (in degrees) (values given in red are data for **2**; values given in blue are data for **4**).

Table 6. Variation of J_{rail} = J(d2) Value as the Geometry of the d2 Radical Pair is Modified, in Three Steps (See Text), and is Converted from 2 (First Column) to the Equivalent Structure of the d2 Radical Pair in 4 (and Vice Versa)

model name	experimental (d2 in **2**)	Step 1	Step 2	Step 3 (d2 in **4**)
model description	d2 experimental geometry in **2**	d2 in **2** setting Cu–Br bond lengths equal to Cu–Cl bond lengths in **4**	d2 in **4** keeping Cu–Br bonding distances as in **2**	d2 geometry in **4** replacing Cl by Br ions
$d_{Cu\cdots Cu}$ (Å)	6.883	6.883	6.903	6.903
$d_{Cu\cdots X}$ (Å)	2.383–2.442	2.248–2.312	2.383–2.442	2.248–2.312
α(Cu–X–Cu) (deg)	92.02	92.02	91.62	91.62
J(d2) (cm^{-1})	−10.26	−10.60	−9.59	−9.72
model name	experimental (d2 in **4**)	Step 1	Step 2	Step 3 (d2 in **2**)
model description	d2 experimental geometry in **4**	d2 in **4** setting Cu–Cl bond lengths equal to Cu–Br bond lengths in **2**	d2 in **2** keeping Cu–Cl bonding distances as in **4**	d2 geometry in **2** replacing Br by Cl ions
$d_{Cu\cdots Cu}$ (Å)	6.903	6.903	6.883	6.883
$d_{Cu\cdots X}$ (Å)	2.248–2.312	2.383–2.442	2.248–2.312	2.383–2.442
α(Cu–X–Cu) (deg)	91.62	91.62	92.02	92.02
J(d2) (cm^{-1})	−8.82	−8.85	−9.41	−9.31

apparent difference in the twist of the 2,3-dmpz rings. Finally, Figure 9b shows the values of the main geometric parameters defining the relative position of the Br and Cl atoms in the bihalide bridge. As observed there, the main change occurs in the Cu–halogen distances.

Once the main change between crystals of **2** and **4** has been shown to be the Cu–halogen distances, it is surprising that the substitution of Cl^- and Br^- ions affects J_{rail} ($|\Delta J_{rail}|_{Br-Cl}$ = 1.60 experimentally and 1.44 theoretically). It is thus worth considering which geometric factors are responsible for the variation of J_{rail} = J(d2) as the geometry of the d2 radical pair is modified from that in **2** to that in **4** (and vice versa). Such change can be envisioned as a set of three successive "hypothetical" steps. In Step 1, the effect of the halogen in J_{rail} will be explored in terms of the Cu–Br distance with a model that uses the geometry of the d2 dimer in **2** with the Cu–Br distances modified to be equal to the Cu–Cl distances that the d2 dimer has in **4** (note there are no changes in the orientation (bond angles) of any of the atoms). In the second step, the structural effect of the crystal packing in J_{rail} will be evaluated with a model that uses the geometry of the d2 dimer in **4** and replaces Cl with Br atoms, preserving the original Cu–Br bonding distances. In the final step, both effects will be considered using a model that is the d2 dimer in **4** and simply replacing the Cl^- ions with Br^- ions.

The results shown in Table 6 enable us to interpret the difference between the values of J_{rail} for **2** and **4** (1.60 cm^{-1} from experiment and 1.44 cm^{-1} from computations). In order to proceed, we will resort to comparison between J values computed using models based in **2** against J values computed using models based in **4**. It is found that this difference can be ascribed to be a cooperative effect, which can be decomposed into one change in J_{rail}, because of the halogen and another change because of the structure. The effect of the halogen can be evaluated comparing experimental d2 in **2** against Step 2 model in **4**: −10.26 cm^{-1} vs −9.41 cm^{-1} (and experimental d2 in **4** against Step 2 model in **2**: −8.82 cm^{-1} vs −9.59 cm^{-1}). The change due to the change in halogen contributes ca. ±0.8 cm^{-1} to the total. It is well-known that, with both terminal and bridging halogens, the polarizing effect of the halogen can influence exchange to the extent that, with Cl, overall charge is localized more within the halide subunits, both bridging and terminal sites, such that exchange is reduced compared with Br (see Table S1 in the Supporting Information). The effect of the structure can be quantified comparing either the experimental d2 in **2** against the Step 2 model in **2** or the Step 1 model in **2** against the Step 3 model in **2**: −10.26 cm^{-1} vs −9.59 cm^{-1}, −10.60 cm^{-1} vs −9.72 cm^{-1}.[51] The change due to the structural effect of the crystal packing amounts to ca. ±0.7 cm^{-1}. The overall effect is ca. ±1.5 cm^{-1}, whose magnitude agrees with the observed $|\Delta J_{rail}|_{Br-Cl}$ value. Therefore, although surprising, the

dx.doi.org/10.1021/ic3005147 | Inorg. Chem. 2012, 51, 6315–6325

substitution of Cl^- ions for Br^- ions does affect the exchange, not only along the rungs but also along the rails of the spin-ladder magnetic topology of **2** and **4**

Finally, we have attempted to explain the difference between the magnetic interactions through the rung ($|\Delta J_{rung}|_{Br-Cl}$ = 0.59 cm^{-1} from experiment and 0.41 cm^{-1} from computations). Calculations of the magnetic interactions by exchanging the halogen anions into the corresponding analogous crystal structure show that, in both cases, the magnitude of the magnetic interaction J_{rung} decreases due to the fact that the overlap between magnetic orbitals from halogens and copper radicals becomes less effective. Accordingly, one can argue that the similar J_{rung} value in both Br and Cl analogues is due to the difference of the anion volume, which produces a separation between copper (pyrazine) chains, i.e., both halogens fit and magnetically bridge equally well, and the halogen size effect is offset by the separation between the Cu ions.

CONCLUSIONS

The synthesis, crystallographic structure at various temperatures, and the magnetic properties of $Cu(qnx)Br_2$ (**1**), $Cu(qnx)Cl_2$ (**3**), and $Cu(2,3\text{-dmpz})Cl_2$ (**4**) are reported. It is found that these crystals are well-described by a two-leg spin-ladder magnetic topology, where $J_{rung} > J_{rail}$, and that these values are similar for both bromide and chloride compounds.

Using the first-principles bottom-up procedure, the magnetic properties of the $Cu(2,3\text{-dmpz})Br_2$ (**2**) and $Cu(2,3\text{-dmpz})Cl_2$ (**4**) crystals are theoretically characterized and compared. These computations confirm that the magnetic topology is a two-leg spin ladder, where $J_{rung} > J_{rail}$ and $|J_{interladder}| \leq 1$ cm^{-1}, and thus there was no need to experimentally explore fitting the data with magnetic models other than the strong-rung spin ladder. The computed values of J_{rung} and J_{rail} (−13.82 and −10.26 cm^{-1} in **2**, and −14.23 and −8.82 cm^{-1} in **4**) are in good agreement with the experiment (−11.03 and −6.39 cm^{-1} in **2**, and −10.44 and −4.79 cm^{-1} in **4**), as well as the computed and experimental magnetic susceptibility curves.

The substitution of Cl^- for Br^- ions does not affect the exchange along the rungs but along the rails of the spin-ladder magnetic topology of **2** and **4**. A comparative study of the rail radical pairs (d2) of **2** and **4** concludes that both the halogen and structural effects change the computed J_{rail} magnetic interaction. In this case, the J_{rail} value for Cl is reduced, compared to Br, because of charge localization within the bridge chloride subunit and at the terminal chloride sites. In contrast, comparison between the rung radical pairs (d1) shows a very small difference in J_{rung}, because of an accidental cancellation of effects: for (**4**), the Cu···Cu distance is shorter than for (**2**), but this is compensated by the larger orbital size in the Br analogue. The final outcome is an almost-equivalent magnetic exchange for J_{rung} in the two analogues.

ASSOCIATED CONTENT

Supporting Information

Dependence of the calculated $\chi(T)$ value on the J_{rung}/J_{rail} relative ratio for **4**. Convergence of calculated $\chi(T)$, depending on the spin-ladder magnetic model size and the interladder exchange models for **2** and **4**. Listing of MSK halogen charges for the tetramer model for **2** and **4**. This material is available free of charge via the Internet at http://pubs.acs.org.

AUTHOR INFORMATION

Corresponding Author

*E-mails: merce.deumal@ub.edu (M.D.), mturnbull@clarku.edu (M.M.T.).

Notes

The authors declare no competing financial interest.

ACKNOWLEDGMENTS

We thank Dr. Fan Xiao for assistance in obtaining the magnetic data and Prof. Shane Telfer for assistance in obtaining the low-temperature data for compound **3**. We are grateful for grants from the NSF (No. IMR-0314773) toward the purchase of the MPMS SQUID, from PCI Synthesis, Inc. toward the purchase of the D8 Powder X-ray Diffractometer, and the Kresge Foundation toward the purchase of both. We thank the economic support of the Spanish Science and Innovation Ministry (Project Nos. MAT2008-02032 and MAT2011-25972 and Ph.D. grant to J.J.S.), the Catalan DURSI (Grant Nos. 2005 PEIR 0051/69, 2005-SGR-00036, 2009-SGR-1203, and EDU/2235/2009 grant to N.C.C.), and the computer time allocated by CESCA and BSC.

REFERENCES

(1) (a) Girtu, M. A. *Magn. Nanostruct.* **2002**, 359. (b) Dagotto, E. *Rep. Prog. Phys.* **1999**, *62*, 1525. (c) Bose, I. *Curr. Sci.* **2005**, *88*, 62.
(2) (a) Schmidt, K. P.; Uhrig, G. S. *Mod. Phys. Lett. B* **2005**, *19*, 1179. (b) Dagotto, E.; Rice, T. M. *Science* **1996**, *271*, 618.
(3) White, S. R. *Phys. Rev. B* **1996**, *53*, 52.
(4) Tranquada, J. M.; Woo, H.; Perring, T. G.; Goka, H.; Gu, G. D.; Fujita, M.; Yamada, K. *Nature (London)* **2004**, *429*, 534.
(5) (a) Uehara, M.; Nagata, T.; Akimitsu, J.; Takahashi, H.; Mori, N.; Kinoshita, K. J. *Phys. Soc. Jpn.* **1996**, *65*, 2764−2767. (b) Nakanishi, T.; Motoyama, N.; Mitamura, H.; Takeshita, N.; Takahashi, H.; Eisaki, H.; Uchida, S.; Mori, N. *Phys. Rev. B* **2005**, *72*, 054520/1−6.
(6) (a) Vuletic, T.; Korin-Hamzic, B.; Ivek, T.; Tomic, S.; Gorshunov, B.; Dressel, M.; Akimitsu, J. *Phys. Rep.* **2006**, *428*, 169. (b) Carter, S. A.; Batlogg, B.; Cava, R. J.; Krajewski, J. J.; Peck, W. F., Jr.; Rice, T. M. *Phys. Rev. Lett.* **1996**, *77*, 1378. (c) Azuma, M.; Hiroi, Z.; Takano, M.; Ishida, K.; Kitaoka, Y. *Phys. Rev. Lett.* **1994**, *73*, 3463.
(7) (a) Yoshida, Y.; Tateiwa, N.; Mito, M.; Kawae, T.; Takeda, K.; Hosokoshi, Y.; Inoue, K. *Phys. Rev. Lett.* **2005**, *94*, 037203/1−4. (b) Kikuchi, M.; Okamoto, K.; Okunishi, K.; Sakai, T. *Prog. Theol. Phys. Suppl.* **2005**, *159*, 251. (c) Sakai, T.; Okamoto, K.; Okunishi, K.; Kindo, K.; Narumi, Y.; Hosokoshi, Y.; Katoh, K.; Inoue, K.; Goto, T. *Physica B: Condens. Matter* **2004**, *346*, 34. (d) Tamura, M.; Hosokoshi, Y.; Shiomi, D.; Kinoshita, M.; Nakasawa, Y.; Ishikawa, M.; Sawa, H.; Kitazawa, T.; Eguchi, A.; Nishio, Y.; Kajita, K. *J. Phys. Soc. Jpn.* **2003**, *72*, 1735.
(8) Ribas, X.; Mas-Torrent, M.; Perez-Benitez, A.; Dias, J. C.; Alves, H.; Lopes, E. B.; Henriques, R. T.; Molins, E.; Santos, I. C.; Wurst, K.; Foury-Leylekian, P.; Almeida, M.; Veciana, J.; Rovira, C. *Adv. Funct. Mater.* **2005**, *15*, 1023.
(9) Wesolowski, R.; Haraldsen, J. T.; Musfeldt, J. L.; Barnes, T.; Mas-Torrent, M.; Rovira, C.; Henriques, R. T.; Almeida, M. *Phys. Rev. B* **2003**, *68*, 134405/1−8.
(10) Deumal, M.; Giorgi, G.; Robb, M. A.; Turnbull, M. M.; Landee, C. P.; Novoa, J. J. *Eur. J. Inorg. Chem.* **2005**, 4697.
(11) Watson, B. C.; Kotov, V. N.; Meisel, M. W.; Hall, D. W.; Granroth, G. E.; Montfrooij, W. T.; Nagler, S. E.; Jensen, D. A.; Backov, R.; Petruska, M. A.; Fanucci, G. E.; Talham, D. R. *Phys. Rev. Lett.* **2001**, *86*, 5168−5171.
(12) Landee, C. P.; Turnbull, M. M.; Galeriu, C.; Giantsidis, J.; Woodward, F. M. *Phys. Rev. B* **2001**, *63*, 100402/1−4.
(13) Willett, R. D.; Galeriu, C.; Landee, C. P.; Turnbull, M. M.; Twamley, B. *Inorg. Chem.* **2004**, *43*, 3804.

(14) Wells, B. M.; Landee, C. P.; Turnbull, M. M.; Awwadi, F. F.; Twamley, B. *J. Mol. Catal. A: Chem.* **2005**, *228*, 117.
(15) Landee, C. P.; Delcheva, A.; Galeriu, C.; Pena, G.; Turnbull, M. M.; Willett, R. D. *Polyhedron* **2003**, *22*, 2325.
(16) Chiari, B.; Piovesana, O.; Tarantelli, T.; Zanazzi, P. F. *Inorg. Chem.* **1990**, *29*, 1172.
(17) Li, L.; Turnbull, M. M.; Landee, C. P.; Jornet, J.; Deumal, M.; Novoa, J. J.; Wikaira, J. L. *Inorg. Chem.* **2007**, *46*, 11254.
(18) Johnston, D. C.; Johnson, J. W.; Goshorn, D. P.; Jacobson, A. J. *Phys. Rev. B* **1987**, *35*, 219.
(19) Barnes, T.; Riera, J. *Phys. Rev. B.* **1994**, *50* (10), 6817–22.
(20) Eccleston, R. S.; Barnes, T.; Brody, J.; Johnson, J. W. *Phys. Rev. Lett.* **1994**, *73*, 2626.
(21) Garrett, A. W.; Nagler, S. E.; Barnes, T.; Sales, B. C. *Phys. Rev. B* **1997**, *55*, 3631.
(22) Garrett, A. W.; Nagler, S. E.; Tennant, D. A.; Sales, B. C.; Barnes, T. *Phys. Rev. Lett.* **1997**, *79*, 745.
(23) Chaboussant, G.; Crowell, P. A.; Levy, L. P.; Piovesana, O.; Madouri, A.; Mailly, D. *Phys. Rev. B* **1997**, *55*, 3046.
(24) Chaboussant, G.; Julien, M. H.; Fagot-Revurat, Y.; Levy, L. P.; Berthier, C.; Horvatic, M.; Piovesana, O. *Phys. Rev. Lett.* **1997**, *79*, 925.
(25) Weihong, Z.; Singh, R. R. P.; Oitmaa, J. *Phys. Rev. B* **1997**, *55*, 8052.
(26) Hammar, P. R.; Reich, D. H. *J. Appl. Phys.* **1996**, *79*, 5392.
(27) Hammar, P. R.; Reich, D. H.; Broholm, C.; Trouw, F. *Phys. Rev. B* **1998**, *57*, 7846.
(28) Butcher, R. T.; Dawe, L. N.; Landee, C. P.; Turnbull, M. M. *Polyhedron* **2009**, *28*, 1710.
(29) Shapiro, A.; Landee, C. P.; Turnbull, M. M.; Jornet, J.; Deumal, M.; Novoa, J. J.; Robb, M.; Lewis, W. *J. Am. Chem. Soc.* **2007**, *129*, 952–9.
(30) Lindroos, S.; Lumme, P. *Acta Crystallogr., Sect. C: Cryst. Struct. Commun.* **1990**, *46*, 2039.
(31) Rigaku. *CrystalClear, Version 1.4.0*; Rigaku Americas Corporation: The Woodlands, TX, 2005.
(32) Rigaku. *PROCESS-AUTO*; Rigaku Corporation: Tokyo, Japan, 1998.
(33) *SMART, Bruker Molecular Analysis Research Tool*; Bruker AXS: Madison, WI, 1997–1998.
(34) *SAINTPlus, Data Reduction and Correction Program*; Bruker AXS: Madison WI, 1999.
(35) Sheldrick, G. M. *SADABS v.2.01: An empirical absorption correction program*; Bruker AXS, Inc.: Madison, WI, 1999.
(36) Sheldrick, G. M. *Acta Crystallogr., Sect. A: Found. Crystallogr.* **2008**, *A64*, 112–122.
(37) Johnston, D. C.; Troyer, M.; Miyahara, S.; Lidsky, D.; Ueda, K.; Azuma, M.; Hiroi, Z.; Takano, M.; Isobe, M.; Ueda, Y.; Korotin, M. A.; Anisimov, V. I.; Mahajan, A. V.; Miller, L. L. arXiv:cond-mat/0001147, 2000.
(38) Deumal, M.; Bearpark, M. J.; Novoa, J. J.; Robb, M.A. J. *Phys. Chem. A* **2002**, *106*, 1299.
(39) From the general Heisenberg Hamiltonian $\hat{H} = -2\sum_{A,B}^{N} J_{AB}\hat{S}A\cdot\hat{S}B$, for a pair of A and B radicals, the J_{AB} value is computed as the energy difference between biradical open-shell singlet S and triplet T states: $\Delta E^{S-T} = E^S - E^T = 2J_{AB}$. The criteria chosen to compute the energy difference is $E^S - E^T = 2(E^S_{BS} - E^T)/(1 + S_{ab})$. Open-shell singlet systems separate alpha spin density and beta spin density on different radicals. In our case, once the broken symmetry approximation is applied, the resulting overlap between the alpha SOMO and the beta SOMO is zero. Thus those orbitals are localized on each of the two radicals. This leads to $S_{ab} = 0$. As a conclusion, $J_{AB} = E^S_{BS} - E^T$.
(40) (a) Noodleman, L. *J. Chem. Phys.* **1981**, *74*, 5737. (b) Noodleman, L.; Davidson, E. R. *Chem. Phys.* **1986**, *109*, 131.
(41) Parr, E. G.; Yang, W. *Density Functional Theory*; Oxford University Press: New York, 1989.
(42) (a) Becke, A. D. *Phys. Rev. A* **1988**, *38*, 3098. (b) Becke, A. D. *J. Chem. Phys.* **1993**, *98*, 5648. (c) Lee, C.; Yang, W.; Parr, R. G. *Phys. Rev. B* **1988**, *37*, 785.
(43) Frisch, M. J. et al., Gaussian 03, Revision C.02; Gaussian, Inc.: Wallingford, CT, 2004.
(44) Alrich's basis set: Schafer, A.; Horn, H.; Ahlrichs, R. *J. Chem. Phys.* **1992**, *97*, 2571–2577.
(45) 6-31+G(d) split-valence basis set: (a) Hariharan, P. C.; Pople, J. A. *Theor. Chim. Acta* **1973**, *28*, 213–222. (b) Francl, M. M.; Petro, W. J.; Hehre, W. J.; Binkley, J. S.; Gordon, M. S.; DeFrees, D. J.; Pople, J. A. *J. Chem. Phys.* **1982**, *77*, 3654–3665.
(46) Szabo, A.; Ostlund, N. S. *Modern Quantum Chemistry*; Macmillan, New York, 1982.
(47) Butcher, R. T.; Novoa, J. J.; Ribas-Ariño, J.; Sandvik, A. W.; Turnbull, M. M.; Landee, C. P.; Wells, B. M.; Awwadi, F. F. *Chem. Commun.* **2009**, 1359.
(48) Turnbull, M. M.; Landee, C. P.; Wells, B. M. *Coord. Chem. Rev.* **2005**, *249*, 2567.
(49) Fitting J values based on $\hat{H} = -\sum_{A,B}^{N} J_{AB}\hat{S}A\cdot\hat{S}B$.
(50) Fitting J values (Table 3) have been translated from original fitting Hamiltonian (ref 49) to the $\hat{H} = -2\sum_{A,B}^{N} J_{AB}\hat{S}A\cdot\hat{S}B$ general Hamiltonian used in the first-principles bottom-up procedure described in ref 38.
(51) The structure effect can also be evaluated using either experimental d2 in **4** against Step 2 model in **4** or Step 1 model in **4** against Step 3 model in **4**: $-8.82\ cm^{-1}$ vs $-9.41\ cm^{-1}$, $-8.85\ cm^{-1}$ vs $-9.31\ cm^{-1}$.